Performance of light fixed-wing airborne time-domain electromagnetic system for mapping the near-surface cover layer in an alluvial plain context: A numerical study

Cyril Schamper, Guillaume-alexandre Sab, Fayçal Rejiba, Nicolas Flipo

Received: 15 April 2022 | Accepted: 25 November 2022

DOI: 10.1111/1365-2478.13306

Geophysical Prospecting | EAGE EUROPEAN ASSOCIATION OF GEOSCIENTISTS & ENGINEERS

ORIGINAL ARTICLE

Performance of light fixed-wing airborne time-domain electromagnetic system for mapping the near-surface cover layer in an alluvial plain context: A numerical study

Cyril Schamper[1] | **Guillaume-Alexandre Sab**[1,2] | **Fayçal Rejiba**[3] | **Nicolas Flipo**[4]

[1]Sorbonne University, Paris Cedex 05, France

[2]Action Air Environnement, S.A.S. Action Communication, Cuers, France

[3]Normandie University, UNIROUEN, UNICAEN, CNRS, M2C, Rouen, France

[4]MINES ParisTech, Centre de Géosciences, Paris, France

Correspondence
Schamper Cyril, Sorbonne University, UMR 7619 METIS, 4 place Jussieu, 75252 Paris Cedex 05, France.
Email: cyril.schamper@sorbonne-universite.fr

Abstract

The mapping of the vertical and lateral variations in the physical properties of the few-meter cover layer over near-surface aquifers is important for hydrogeological modelling, particularly for the quantification of the recharge of groundwater systems. The first ground-based time-domain electromagnetic survey over a small catchment (Avesnelles, France) of the watershed of Orgeval (Seine basin) was carried out to determine discontinuities in the first silt layer as well as in the Brie multilevel aquifer limestone horizon. The results highlighted the following: (1) a good sensitivity of the time-domain electromagnetic survey to the presence of multi-decametric resistive sand lenses, particularly in a location where they were previously identified and (2) the interest in conducting a survey at a fine sampling step but extending to the meso-scale. To overcome the sampling issue over a watershed of several hundred square kilometres, we proposed numerically assessing the use of a prototype of low-cost airborne transient electromagnetic systems towed by light fixed-wing airplanes (with transmitting and receiving loops in the same plane). The present numerical analysis, in 1D for the vertical (i.e. thickness) variation and in 3D for the lateral extensions of localized sandy and resistive units, showed that a conductive few-meter cover can be mapped even with a system flying at 50 m with, however, the need of a priori constraint on the resistivity of the first layer to estimate its thickness variation as accurately as possible. Even if it did not bring more sensitivity to the layer thickness and despite the severe difficulty of practical implementation with a decametric emission loop, the vertical co-planar configuration potentially offered better near-surface lateral resolution (down to ∼40 m) to delineate the sandy units (discontinuities) within the silt layer (if units are at least 50 m in size) and provided better spatial constraints compared to the classical horizontal co-planar geometry used in the time-domain electromagnetic. Even if not aerodynamically in the plane of the emission loop, the measurement of the H_x component with a vertical dipole emission loop (PERPxz geometry for perpendicular) improved the lateral resolution (down to ∼20 m; still with at least 50 m size sand units) and confirmed that a geometry different from the classical horizontal co-planar configuration could be valuable.

KEYWORDS
electromagnetic modelling, hydrogeophysics, time-domain electromagnetic

INTRODUCTION

Time-domain electromagnetic (TDEM) systems, similar to other airborne electromagnetic (AEM) techniques, are widely used as the primary exploration technique within the mining industry and for hydrogeological prospection. A wide range of TDEM and frequency-domain electromagnetic (FEM) systems have been developed for these purposes. Airborne TDEM technology appeared 70 years ago, with the first successful flights being made by Stanmac Ltd. and McPhar Geophysics Ltd. (Fountain, 1998). Until the late 1990s, technical improvements were focused on the moment (or power) of the transmitter systems, which were optimized to reach larger depths than those reached by FEM systems, which at low frequencies are limited by the minimum source-receiver offset required to ensure reliable recording of the signals from the ground. At that time, the performance of airborne TDEM systems for the investigation of near-surface features was relatively poor compared to FEM systems (Allard, 2007; Steuer et al., 2009). Since the 1990s, technical developments have mainly focused on electronics and processing, as discussed by Macnae (2007), Nyboe and Sørensen (2012) and Thomson et al. (2007). Improvements in short time delay (commonly referred to as 'early time') acquisition and inversion techniques finally improved TDEM to a level comparable with that of FEM in terms of lateral and vertical resolutions (Bedrosian et al., 2016).

Helicopter-borne TDEM systems have already shown their ability to produce images of near-surface (less than 100-m depth) sedimentary hydrosystems (e.g. Schamper, Jørgensen, et al., 2014; Sorensen & Auken, 2004). However, the cost of AEM surveys is a non-negligible bottleneck for many hydrogeological projects, particularly in developing countries. In the national French TEMas project 2014–2017 (transient electromagnetic airborne sensor, a project developed by the PEGASE competitiveness cluster for the FUI 16 program), a new prototype of an airborne TDEM device was developed to be towed by a light fixed-wing aircraft (single engine). The towed antenna was expected to fly approximately 50 m above ground level. This is lower than the minimum flight height of existing fixed-wing systems (~100 m), which are not allowed to fly in Europe for safety regulations, but higher than helicopter-borne EM systems (~30 m). Therefore, the device was designed to operate between these two heights. An interesting possibility for a TEMas-like device (Sab, 2017) is to set up the antennas in a vertical co-planar (VCP) configuration instead of the classical horizontal co-planar (HCP) geometry. The VCP configuration is well known to be more sensitive to lateral changes and near-surface features in the frequency domain (e.g. Guillemoteau & Tronicke, 2015) and for TDEM device of metric size (Thiesson et al., 2007). As the VCP configuration has never been considered for large TDEM systems, this study is an attempt to analyse its performances for the hydrogeological context and targets considered. The H_x component (horizontal and perpendicular to the axis of the magnetic source dipole), also called the in-line component (called perpendicular 'PERPxz' configuration in the frequency domain) and regularly used in mining exploration to better constrain 3D inversion (e.g. Cox et al., 2012), is also analysed.

The paper begins with a section that describes the Orgeval basin site and an example of ground-based geophysical survey on the Brie Plateau. The results from the electrical resistivity tomography and ground-based TDEM surveys and geological models for 1D and 3D analyses were obtained using the inversion method. The first numerical study focused on the thickness variation of the loess cover through 1D modelling with normalized differences calculation of the forward TDEM responses and equivalence analysis. The second analysis concerns local sandy inclusions and is therefore carried out with 3D modelling by mapping normalized differences over the survey area and assessing the capability to distinguish two close anomalies to determine the expected lateral resolution. Both studies were conducted within the context of the Orgeval basin by considering the technical specifications and limitations of a light fixed-wing TDEM system with a TEMas-like configuration (Sab, 2017).

NEAR-SURFACE GEOLOGICAL CONTEXT

Currently, for regional-scale areas of hundreds of km^2 and multi-decametric depth investigations, only airborne geophysics can characterize the near-surface geological variability, particularly electromagnetic induction methods (e.g. Siemon et al., 2020). To evaluate the performance of the airborne time-domain electromagnetic (TDEM), a numerical model was derived from the Orgeval experimental basin located 70 km east of Paris (Tallec et al., 2015). The Orgeval basin, with an area of 104 km^2, is characterized by intensive agriculture on 80% of its area; in fact, it is particularly representative of the agricultural watershed of the central Paris Basin (Tallec, 2012). The Orgeval basin is connected to a multilayered aquifer system (Mouhri et al., 2013): (1) cover of low-permeability loess of 2–5 m thickness, (2) primary aquifer: Oligocene (sand and limestone), (3) clayey aquitard composed of mudstone and marl and (4) secondary aquifer: Middle Eocene (limestone). An example of the geology for

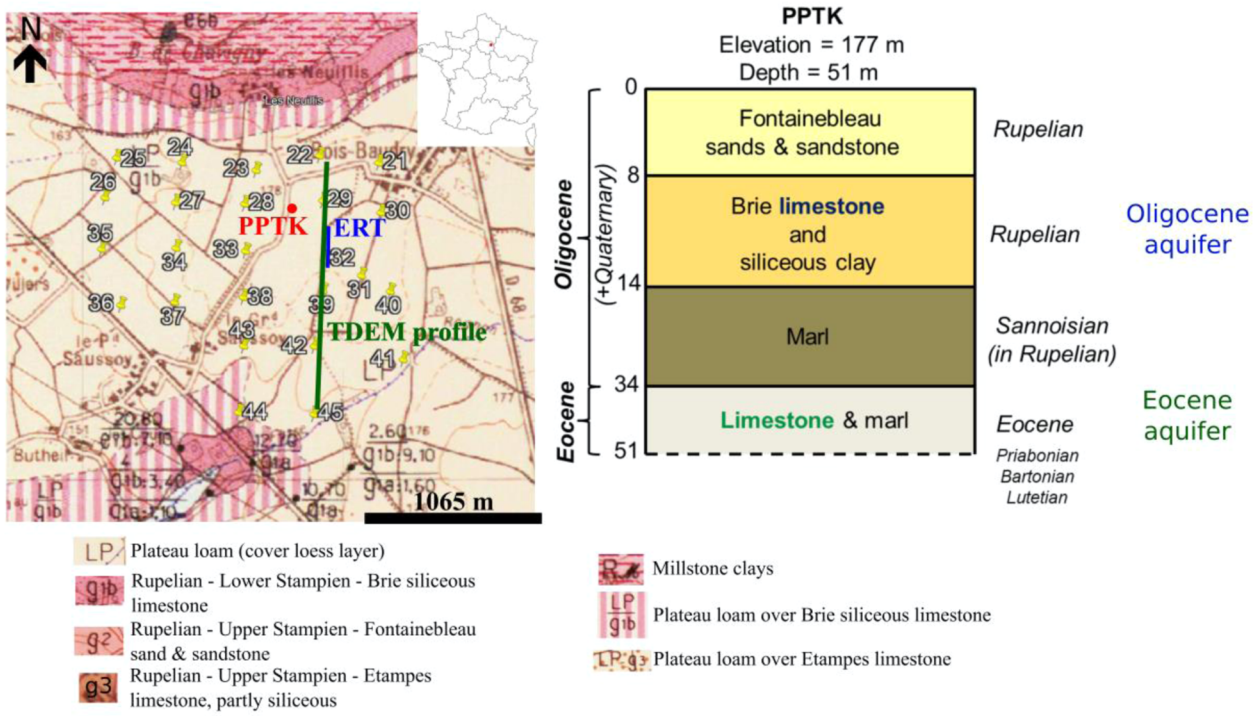

FIGURE 1 Geological context on the Brie Plateau of the Orgeval basin with geological map and log (from the BRGM InfoTerre database). Time-domain electromagnetic (TDEM) soundings are indicated as yellow pins and electrical resistivity tomography (ERT) as a blue line. The formations corresponding to Oligocene aquifer are indicated in blue text, and the ones to Eocene aquifer in green text on the geological log.

a sub-area of the basin on the Brie Plateau is illustrated in Figure 1. The hydrogeological function of the Orgeval basin is constrained by these two main aquifers. Its conceptual modelling involves two main unknowns:

1. In some places, there are 1D uncertainties concerning the thickness variations of 'high electrical conductivity and low permeability' loess cover which is visible on the geological map of Figure 1 ('LP' formation), but not on the geological log 'PPTK' of the area. The presence of this thin loess cover is confirmed in the geophysical sections of Figure 2.
2. In other places, the loess cover shrinks and is locally replaced by loam and sand lenses with significantly lower electrical conductivities (3D uncertainties) and higher hydraulic conductivities, as illustrated by the Rupelian sand units visible in the electrical resistivity tomography (ERT) of Figure 2b. Consequently, 3D uncertainties regarding the presence of these sand lenses connected to the primary limestone aquifer constitute a critical issue in the modelling of groundwater flows.

These two types of near-surface variabilities, that is the thickness of lithological layers and the spatial distribution of sandy lenses in the Oligocene near-surface aquifer system, must be accounted for in regional hydrogeological models, regardless of their resolution and scale. In the geological context of the Orgeval basin, the direct current electrical resistivity allows significant discrimination between all types of geological formations with a limited influence of the water table located in the cover layer constituted by the conductive loess formation (Mouhri et al., 2013), just below the ground surface. Considering all formations as saturated and the results of the ground-based survey (Figure 2), the resistivity of sand lenses lies in the 100–300 Ω m range, for limestones in the 40 Ω m range, for loess in the 10–40 Ω m range and for clayey formations below 20 Ω m.

Extensive ground-based geophysical studies over the Orgeval basin have been performed to improve the geometrical characterization of both Oligocene and Eocene aquifers (Mouhri et al., 2013). Based on ERT and TDEM ground-based surveys (a part is shown with locations in Figure 1 and with inversion results in Figure 2), a theoretical analysis of an airborne light fixed-wing TDEM system is proposed concerning (1) the capability of following the thickness of the loess cover defined as a 1D layer, and (2) the sensitivity to very resistive (hundreds of Ω m) sand lenses inside the loess layer. The geometry of the system considered was inspired by the specifications set during the TEMas project (Sab, 2017), the purpose of which was to design a low-cost prospection system while still allowing good performance in the resolution of the first tens of meters. As presented later in this paper, this system allows for the possibility of acquiring in the vertical co-planar mode, whereas all airborne TDEM systems only

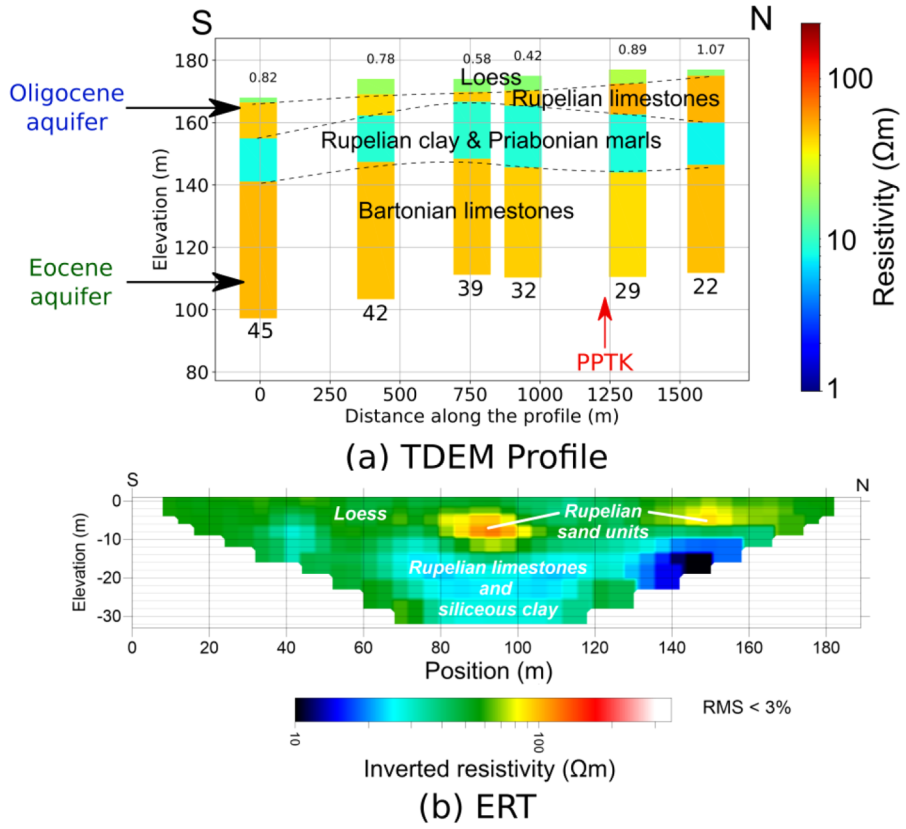

FIGURE 2 Ground-based geophysical results (locations in Figure 1): (a) inversed time-domain electromagnetic (TDEM) profile (survey was performed using TEMFAST with a coincident loop of 25 × 25 m). Normalized residual is indicated above each sounding. A geological interpretation is proposed based on the log in Figure 1. Geological log 'PPTK' is located by a red arrow. Soundings are truncated below a depth of investigation estimated after inversion (Christiansen & Auken, 2012); (b) inversed electrical resistivity tomography (ERT) results (Syscal Pro, Iris Instruments, with Wenner–Schlumberger arrays and 96 electrodes with a 2-m spacing). Proposed geological interpretation is indicated in white. Displayed elevations are relative.

TABLE 1 Tabular resistivity model based on the Orgeval basin context

Resistivity (Ω m)	Thickness (m)	Lithology
15	0–5	Cover loess layer
40	10	Sand and limestone Oligocene aquifer
7	20	Mudstone and marl clayey aquitard
40	–	Limestone middle Eocene aquifer

allow in the horizontal co-planar mode (plus the measurement of x and y magnetic components in some 3D studies; e.g. Smith & Keating, 1996).

Based on the geological information (Figure 1) and the geophysical results (Figure 2), an average 1D model representing the four geological layers (loess cover, Oligocene aquifer, Rupelian clay and Eocene aquifer) is proposed in Table 1 and is considered for the 1D analysis. The loess layer is included in the model despite it is not mentioned in the geological log of Figure 1. This layer can be inexistent locally and is visible in the geophysical sections of Figure 2.

On the ERT profile (Figure 2b), two resistive inclusions (associated to sandy units) were located in the first tens of meters with decametric lateral extension. It can be noticed that these inclusions are not visible on the TDEM profile (Figure 2a), as the average spacing between soundings for this ground-based survey was only 200–300 m. Evaluation of the potential of an airborne TDEM survey, for which a denser sampling along a flight line can be obtained, is therefore of high interest. As the focus of the present paper was the sensitivity analysis of superficial anomalies, 3D sandy units of 300 Ω m over the first 5 m (of the 1D model presented in Table 1) were considered for the 3D lateral sensitivity analysis.

METHODS

Airborne time-domain electromagnetic acquisition parameters

The planned fixed-wing system illustrated in Figure 3a was expected to fly at a ground speed of approximately 100 km/h

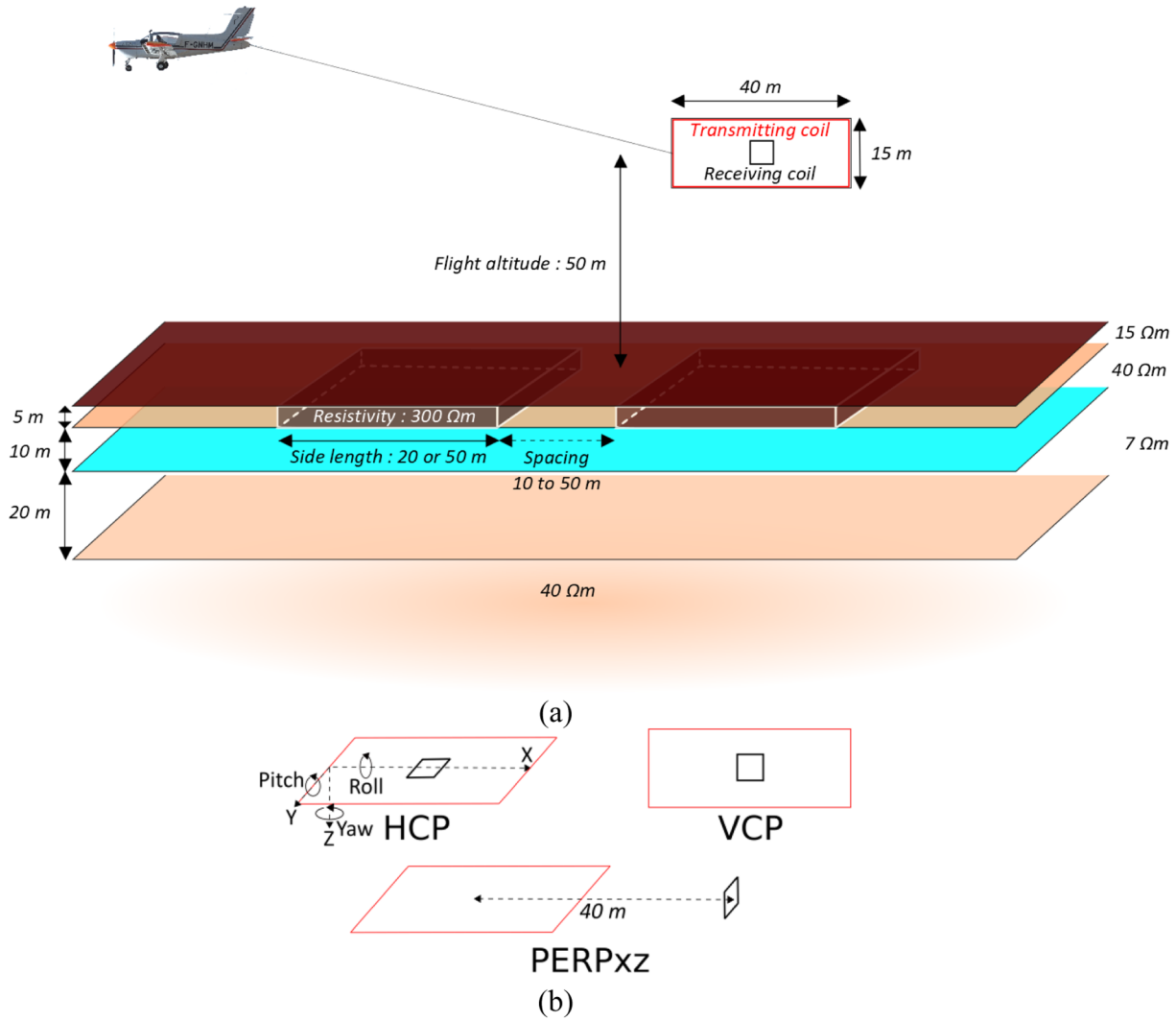

FIGURE 3 Configurations tested for the 1D and 3D sensitivity analysis: (a) 3D resistive inclusions in the surface cover layer. Spacing between the two bodies is varied to quantify coalescence and lateral resolution; (b) acquisition geometries tested of the 1D and/or 3D analysis

with the acquisition system at a nominal altitude of 50 m, which is higher than that of helicopter-borne time-domain electromagnetic (TDEM) systems (~30 m) but lower than that of other fixed-wing systems using larger airplanes (closer to 100 m). Figure 3b summarizes the acquisition geometries that will be considered for the sensitivity analysis in 1D and/or 3D (PERP*xz* configuration only for 3D).

Because the focus was on near-surface ground, the lateral resolution, and therefore sampling, was of critical importance. The observation period for each pulse must be sufficiently short so that the stack operation is not carried out over an extremely long distance (which should not exceed the size of the transmission loop, here 40 m for the longest side). As injecting current during a longer time ('on period') than the observation period (or 'off period') does not bring much more sensitivity in depth (Sab et al., 2014), the duty cycle was set to 50%, that is the pulse duration was equal to the observation period. A period of 2 × 1 ms × 2 (negative and positive pulses) is a good compromise and corresponds to a distance of 0.11 m, which allows a stack window of more than 500 raw soundings over a distance of 30 m. This shows a sounding distance that is clearly lower than the best expected resolution for a 40 m × 15 m T_x loop flying at an altitude of 50 m.

The prototype development led to a turn-off time of 10 μs for a current of 50 A. The moment of the system was also quite low (30,000 Am^2); other existing airborne electromagnetic systems easily provide several hundred thousand Am^2 and even reach a few million Am^2 for the largest ones (e.g. Sørensen et al., 2013). Because this study focused on the first tens of meters, no larger moment value was considered.

A cut-off frequency above 400 kHz was measured on the Rx prototype antenna. However, to avoid variations in the cut-off frequency owing to changes in the average ground resistivity, we decided to fix the low-pass filter at a lower frequency of 350 kHz.

As the Rx antenna is perturbed by the residuals of the primary field just after the current ramp-off, which is particularly the case for a central and off-ground TDEM configuration,

TABLE 2 Configuration of the airborne time-domain electromagnetic (TDEM) device considered (for both horizontal co-planar [HCP] and vertical co-planar [VCP] geometries)

Pulse duration	1 ms
Observation period	1 ms
Turn-off time of the linear ramp	10 μs (3 μs tested)
Flight altitude	50 m
T_x size	40 m × 15 m × 1 turn
Intensity injected	50 A
Moment	30,000 Am^2
Rx	Central
Low-pass filter cut-off frequency	350 kHz

a bucking coil was considered when designing the prototype for the first field tests on the ground. The set-up of such a coil remains critical for being able to exploit the data at early times, even more when the ground is resistive. However, the consideration of its efficiency cannot be done without field tests in air, as it is very sensitive to the precise positioning of the bucking coil in relation to the T_x loop. The modelling of the bucking coil is therefore not considered in the present paper, which is equivalent to have a perfect bucking coil.

The technical characteristics are summarized in Table 2.

For the 3D sensitivity analysis, the acquisition settings were identical to those used for the 1D analysis. To map the 3D heterogeneities, a sounding grid of 30 × 30 m was considered. Although the line spacing is commonly larger than the sounding spacing along the flight lines, the grid was considered uniform to take into account any possible direction of the flight lines chosen before the survey. A discussion of the results would consider a more realistic value of at least 100 m between the flight lines in one direction. Considering an average ground speed of 100 km/h and an acquisition frequency of 250 Hz (successive negative and positive pulses), each sounding corresponded to a stack window of approximately 270 raw soundings (or 540 negative and positive pulses) for a period of 1 s.

Forward modelling of TDEM response in 1D and 3D

In the present modelling, the transmitter coil was approximated by a succession of electric dipoles. In the horizontal co-planar (HCP) configuration, the response to the transmitter loop was computed by summing the analytical solutions for horizontal electric dipoles; in the vertical co-planar (VCP) configuration, vertical electric dipoles must also be considered.

Analytical solutions for the frequency domain can be found in Ward and Hohmann (1988). The Hankel transforms were evaluated using the numerical filters developed by Guptasarma and Singh (1997). These filters were shown to be sufficiently efficient and accurate for frequencies below a few hundred kilohertz, particularly when the offset (distance between the transmitting and receiving coils) was less than 100 m.

An inverse Laplace transform was then used to translate the results into the time domain. More precisely, the Fourier sine expression of the inverse Laplace transform based on the imaginary part of the frequency response was used to compute the response to a unit step function (Mitsuhata et al., 2001). The computational algorithm based on the use of digital filtering was described in detail by Anderson (1982). Fitterman and Anderson (1987) revealed the effect of transmitter turn-off on the ground transient response. To consider this parameter, as well as the on-time duration, the full pulse was described by a piecewise linear waveform.

Finally, the high-frequency content is damped by all TDEM systems, whose cut-off frequency depends on the geometry of the receiver coil, transmitter waveform, and subsurface resistivities. Although damping is inevitable, because of the large dimensions of TDEM systems, the filtering of radio frequency emissions can improve the signal-to-noise ratio of late time-delay recordings. Thus, an electronic low-pass filter (set to 350 kHz) was included in the system to stabilize the cut-off frequency of the system to a fixed value, regardless of the resistivity of the ground. This was designed to impose a constant cut-off frequency below the frequency range induced by variations in the ground resistivity. The behaviour of analogue electronic filters was modelled digitally using a first-order Butterworth filter (Effersø et al., 1999).

For the 3D analysis, the so-called (semi-analytical) method of moments (MoM) model was considered to be the most relevant method for this application, as it allowed only the 3D domain of the target(s) to be discretized and the numerical electromagnetic response to be superposed onto the analytical solution for a tabular ground. The numerical codes developed by Schamper et al. (2011, 2012) for modelling frequency EM response in 3D were used with the addition of frequency-to-time-domain conversion, as described for 1D modelling. The same Green kernel functions have been used for the 1D inversion of a TDEM ground-based survey with TEMFAST device in Tunisia (Finco et al., 2018). A detailed theory of the MoM can be found in Hohmann (1975). To compute the volume integral, the 3D body volume was discretized into cuboids that were smaller than the wavelength of the source (Tabbagh, 1985). Considering a cut-off frequency of 350 kHz, cell gridding of 5 × 5 × 1 m was considered.

The analysed heterogeneities were two parallelepipeds of 50 × 50 m (or 20 × 20 m) and 5 m thickness, which represent two resistive inclusions of 300 Ω m within the conductive cover layer of 15 Ω m (Figure 3a). These resistive inclusions would correspond to sandy units with high hydraulic permeability compared to the loess cover layer. Their localization is

of high importance when studying water infiltration from the ground to underlying aquifers. Their detection with inductive EM methods is also a challenge, as electrically resistive targets embedded in a conductive environment generate lower inductive responses compared to conductive targets.

Assessing near-surface sensitivity in TDEM signal

In the present study, the difference between two TDEM signals was quantified by a normalized residual term (which has no unit) and was calculated as

$$\text{Residual}\left(D_s,\ D_r\right) = \sqrt{\sum_{i=1}^{N_t} \frac{\left(D_s\left(i\right) - D_r\left(i\right)\right)^2}{\left(D_r\left(i\right) \times \text{STD}f\right)^2} \Big/ N_t}, \quad (1)$$

where N_t is the number of time gates (the same value is used for the studied and reference signals); $D_s(i)$ and $D_r(i)$ are the db/dt data for the studied and reference signals, respectively, for the ith time gate; and STDf is the standard deviation factor representing the measurement uncertainties. A residual <1 indicates that the two signals are identical within the STD error bars.

A minimum and not too optimistic relative error of 5% was considered for all gates. Despite its almost negligible influence (as the present study focuses on the very near-surface), a noise level at late times was considered. Munkholm and Auken (1996) showed that the noise slope after log-gating was −1/2 in log–log space. These results were used to simulate white noise using an affine function in log–log space, with a slope equal to −1/2 and a chosen signal level of 1 ms. This allowed the STD errors to be estimated at late times. The HCP noise was set to 5.10^{-9} V/m^2 at 1 ms. Field feedback about the noise level for horizontal magnetic components is less numerous in the literature than for the vertical component. Some authors (e.g. Auken et al., 2007) have reported noise levels 8–10 times higher than the vertical component. In the present simulations, we used the most pessimistic value (i.e. 10 times) for the VCP noise level, so 5.10^{-8} V/m^2 at 1 ms.

If a low computation time is consumed, sensitivity analysis based on linearization and the Jacobian matrix does not highlight the inevitable issue of resolution and equivalence. As a four-layered model was considered, meaning seven model parameters, a systematic analysis over the entire range for each parameter would have been time-consuming. The neighbourhood algorithm of Sambridge (1999) was adapted for this analysis. At the first iteration of the algorithm, the models parameters (for a population of several tens of thousands initial models, here 20,000) are quasi-randomly chosen over user-defined ranges following a uniform distribution law. After the computation of the forward TDEM responses of these first test models and calculation of the residuals in comparison to the reference studied model, the algorithm selects the Voronoï cells around the models where the residuals are the lowest (the number of cells considered is a user-defined parameter, here set to 400 cells in which 1200 new models are generated). Then at the second iteration, the algorithm generates new test models (a user-defined number too) within the selected Voronoï cells to focus the search within the 'best' areas. TDEM responses of these models are computed and compared to the response of the reference model. New Voronoï cells are therefore created, and the algorithm continues to refine where the residuals are the lowest at the next iterations. After a certain number of iterations, the Voronoï cells become very small and the algorithm stays stuck at the same models. The different user-defined parameters mentioned have to be fine-tuned so that the algorithm is set in an 'exploration' mode rather than a 'fast converging' one which would be equivalent to a deterministic quasi-linear inversion. Therefore, the numbers of test models and of Voronoï cells have to be not too small in order to explore the model space as completely as possible, despite it increases the computation time (the order of an hour). Five different runs with the search parameters set as above were carried out in order to maximize the coverage of the equivalence space. As a seven-dimensional space was quite large, especially if all possible resistivity or thickness values were considered, a minimum of a priori information was also considered with likely parameter ranges specific to each lithological layer. The parameter ranges are presented in Table 3.

TABLE 3 Ranges of the parameters studied in the equivalence analysis

Parameter	Min. value	Max. value
ρ_1	5	30
ρ_2	10	200
ρ_3	1	20
ρ_4	10	200
t_1	0.1	10
t_1	0.1	20
t_3	0.1	40

Note: Resistivities ρ are in Ω m and thicknesses t in m.

RESULTS

1D sensitivity analysis: thickness variations of the cover layer

Residual analysis

Before carrying out a sensitivity analysis regarding the thickness of the cover layer through the exploration of the

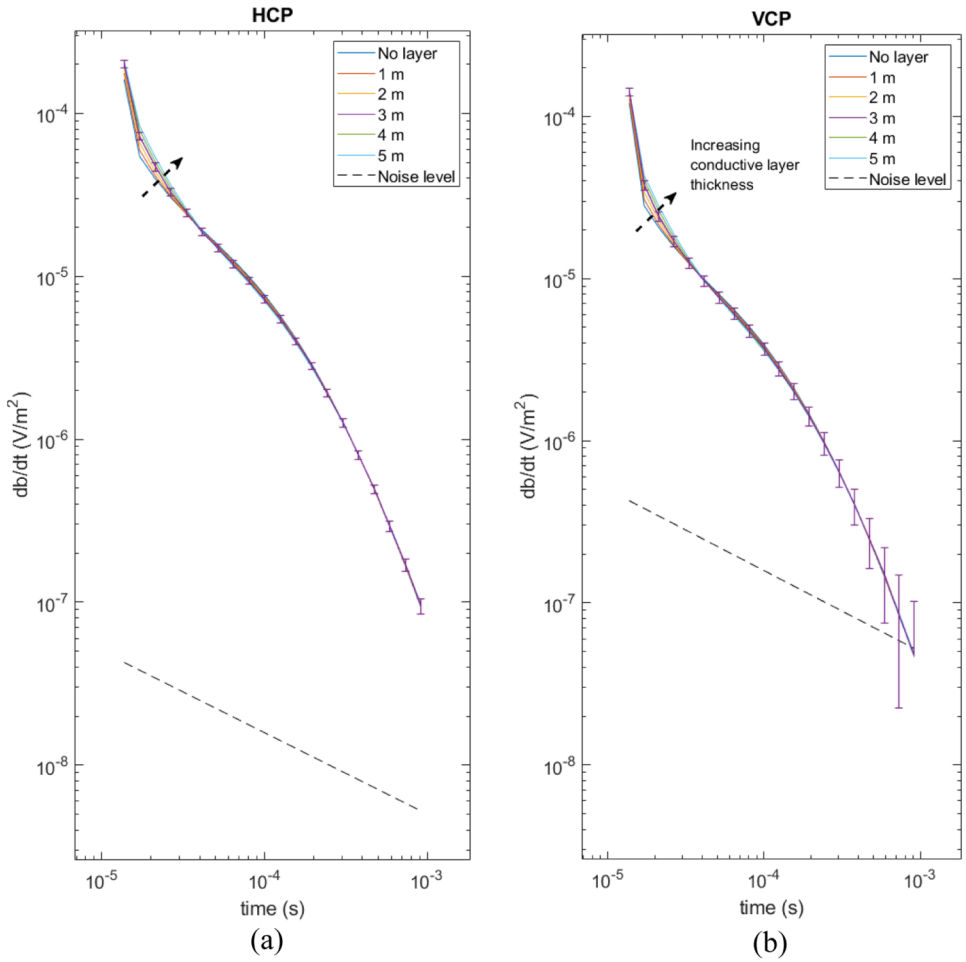

FIGURE 4 Time-domain electromagnetic (TDEM) responses for (a) horizontal co-planar (HCP) and (b) vertical co-planar (VCP) configurations with their corresponding noise curves decreasing as a factor of $t^{-1/2}$. Effect of the change in the thickness of the cover layer (first layer of model detailed in Table 1) is visible at early times.

equivalence space, it was important to verify that modifying the near surface had an impact on the time-domain electromagnetic (TDEM) response itself. Figure 4 shows the TDEM response for different layer thicknesses, from 0 ('No layer') to 5 m. This illustrates that most of the information regarding the cover layer was contained in the first 30 μs for both the horizontal co-planar (HCP) and vertical co-planar (VCP) configurations. For both configurations it can be observed that the system response due to the consideration of a low-pass filter of 350 kHz induces a very quickly decreasing curve at the first two gates. Because of the lower VCP signal compared to HCP one, it also implies that the TDEM response of the conductive cover layer response is more masked by the system response for VCP (Figure 4b) compared to HCP (Figure 4a).

To quantify these visual differences, the residual is plotted in Figure 5a, with the cover layer not included in the reference model. A 1-m thickness generated a residual lower than 1 and was therefore expected to not be mapped. From a thickness of 2 m, the residual became higher than 1 and close to 1.5, which started to be non-negligible. The slightly lower residual for VCP compared to HCP was due to the impact of the low-pass filter of 350 kHz which had a preponderant effect on the lower VCP signal.

Could different thicknesses be distinguished between each other? Figure 5b shows the evolution of the residual with the reference model containing a 1-, 2-, 3- or 4-m thinner cover layer. It clearly appears that a difference of 1 m was not expected to be sensed for both HCP and VCP configurations, which behaved similarly with curves very close each other. From a thickness difference of 2 m, the variation in the TDEM signal was detectable with a normalized residual above 1. The low-pass filter had again an effect for the thinnest layers, as the TDEM response of those layers appeared at earlier gates compared to the thicker layers, which implied a slight decrease of the residual (Figure 5b).

The similar sensitivities for HCP and VCP configuration regarding the thickness variation of the near-surface cover layer were surprising, as it is known for a while (particularly for ground-based measurements in the frequency domain) that VCP has a better sensitivity to very near-surface

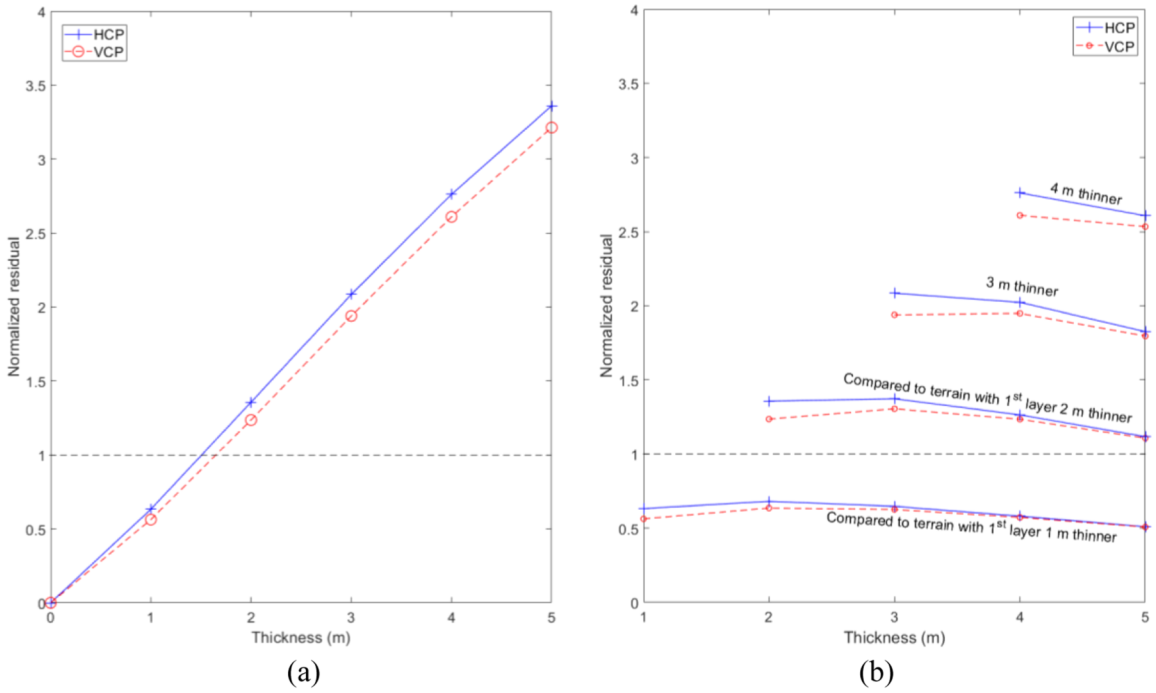

FIGURE 5 Residual between time-domain electromagnetic (TDEM) responses with varying thicknesses of the first 15 Ω m conductive layer: (a) the residual compared to the ground without the cover conductive layer and (b) the residual compared to ground models with thinner first layer

layers compared to HCP configuration which in the other hand allows deeper investigations (McNeill, 1980). Similar plots (not shown in the present paper) were generated for lower (impractical in practice) altitudes of 10 and 20 m, and it illustrates that the VCP sensitivity, if better than HCP one at very low altitudes (especially if low-pass filter of 350 kHz is not considered), actually converges to HCP sensitivity when the altitude increases.

Equivalence analysis

For both HCP and VCP configurations, the results of five different runs were gathered to obtain representative statistics. For both HCP and VCP, this resulted in more than several hundred thousand equivalent models, including all degrees of model proximity. The identified equivalent models (with a normalized residual <1) are displayed in Figure 6 (models with a residual >1 are shown in grey). The thickness of the cover layer for the reference model was 5 m. The envelope of the equivalent models illustrates the margins of uncertainty of the resistivity and thickness values, which were the same for HCP and VCP as presumed when looking at the forward responses in Figure 4.

This analysis concludes that (1) VCP at an altitude of 50 m did not provide a better vertical resolution compared to HCP; (2) the good determination of the 5-m cover layer, more precisely of its thickness, required a priori constraint on its resistivity (e.g. with the help of local electrical resistivity tomography [ERT] measurements).

Sensitivity to pitch and roll

Device shown in Figure 3a is likely to rotate while flying in air. Two types of rotation can disturb the measurements for both 1D and 3D ground structures: the pitch around the *Y* axis, which makes the loop tilting down or up; and the roll around the *X* axis, which makes the loop turning around its principal axis (Figure 3b). The yaw around the *Z* axis has an impact when dealing with 3D or at least lateral variations, as this rotation is going to change the main orientation and the location of the loop while remaining at the same altitude and in the same horizontal (for HCP) or vertical (for VCP) plane. Maintaining the best possible the trajectory of the loop in the axis of the flight line is crucial for 3D studies. However, it does not prevent from monitoring the position of the loop in the air with several GPS antennas, in order to properly consider the orientation of the loop locally when inverting in 3D.

Pitch and roll effects can be easily estimated with 1D modelling. Figure 7 illustrates the impact of the roll. By rotating around the *X* axis, the transmission loop generates a primary field as a combination of horizontal and vertical magnetic dipole sources, and the measured field is also a combination of vertical and horizontal (*Y* axis) components. For the estimation of the perturbations induced by the roll, the altitude of

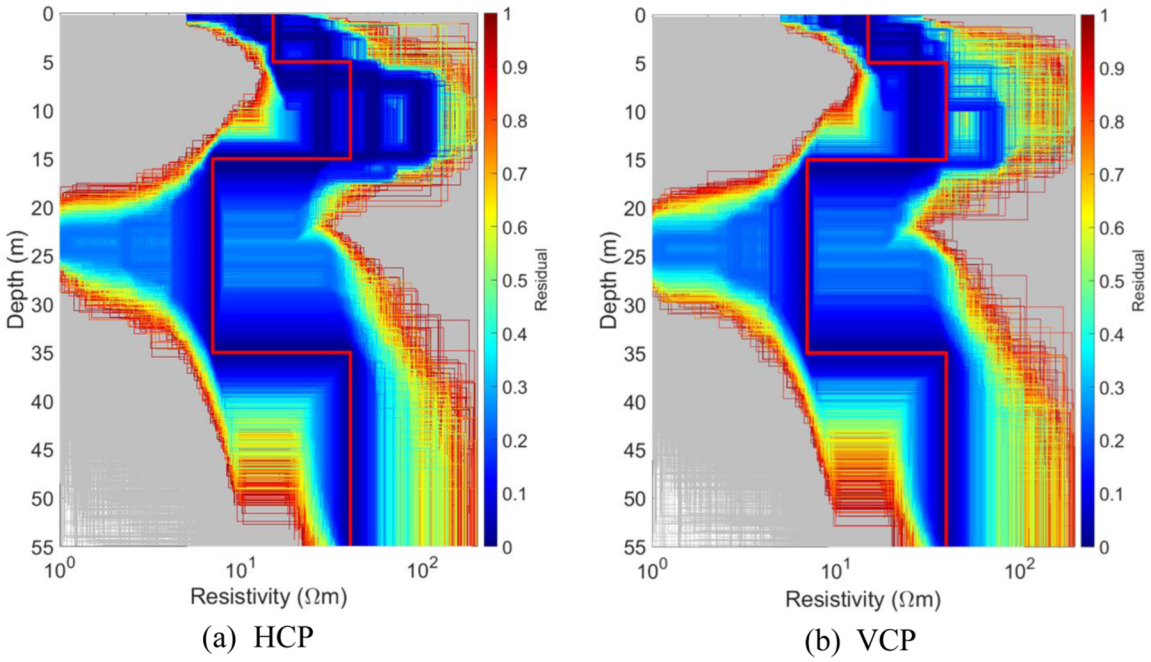

FIGURE 6 Equivalent models (residual <1) compared to the reference model (red line) with a 5 m thick cover layer (red line): (a) horizontal co-planar (HCP) configuration; (b) vertical co-planar (VCP) configuration. Tested models corresponding to residuals >1 are shown in grey. The acquisition configuration is summarized in Table 2.

the device is considered stable at 50 m. To better quantify the differences visible in the forward responses of Figure 7a, the normalized residual compared to the initial HCP or VCP configuration is computed in Figure 7b. It shows that differences start to be non-negligible (i.e. residual >1) when roll values exceed around 20° (a little bit less for VCP).

For estimating the perturbations due to pitch, the combination of vertical and magnetic dipole sources and measured components is also considered, but with the addition of an altitude change (of the centre of the transmission loop), which is positive or negative depending if the device tilts up or down. For the VCP configuration, only altitude change is considered as the loops remain within the same vertical plane. Figure 8 shows that perturbations due to pitch are non-negligible from lower values of rotation compared to roll (Figure 7), from 5° to 10°. Measurements are therefore more sensitive to pitch.

Even if a roll up to 20° seems acceptable, both roll and pitch have to be monitored with inclinometers during acquisition in air in order to correct or reject the data.

3D sensitivity analysis: lateral heterogeneities of the cover layer

Coalescence and expected lateral resolution

Assessing the connectivity between inclusions is related to the lateral resolution capabilities of the airborne TDEM system. In the present case, we considered a simple but representative configuration with a spacing between the two inclusions, which varied from 10 to 50 m. As anticipated, the individual EM responses of the two bodies merged into a single EM anomaly when the spacing became very small (coalescence phenomenon). Figure 9a,b shows the residual maps for HCP and VCP configurations and for the 50 m × 50 m and 50 m spacing cases. It can be observed that for this maximal spacing, the two VCP anomalies (Figure 9b) are clearly more distinguishable from each other compared to the HCP case (Figure 9a), for which only a single maximum exists at a mid-distance between the two bodies. In addition, the area where the normalized data residual is above 1 is larger for the VCP than for the HCP. Figure 9c,d corresponds to the 20 × 20-m size case. For this size, neither the HCP nor the VCP configuration was able to detect the sandy units.

Figure 10 illustrates the other smaller body spacings with the residual profile at $Y = 0$ m. Similar observations with the 50-m side bodies could be made for the 40-m spacing case, that is two maximums for VCP with larger residual values than for HCP. From 30 m and below, the VCP residuals no longer showed two maxima, but the local residual remained larger than that of the HCP configuration. Figure 10c,d confirms again that the 20-m side bodies could not be detected for both configurations.

Regarding the 50-m side bodies, the overall residuals for the VCP configuration were noticeable (>1) in a larger area compared to HCP, for which the data residual might have been

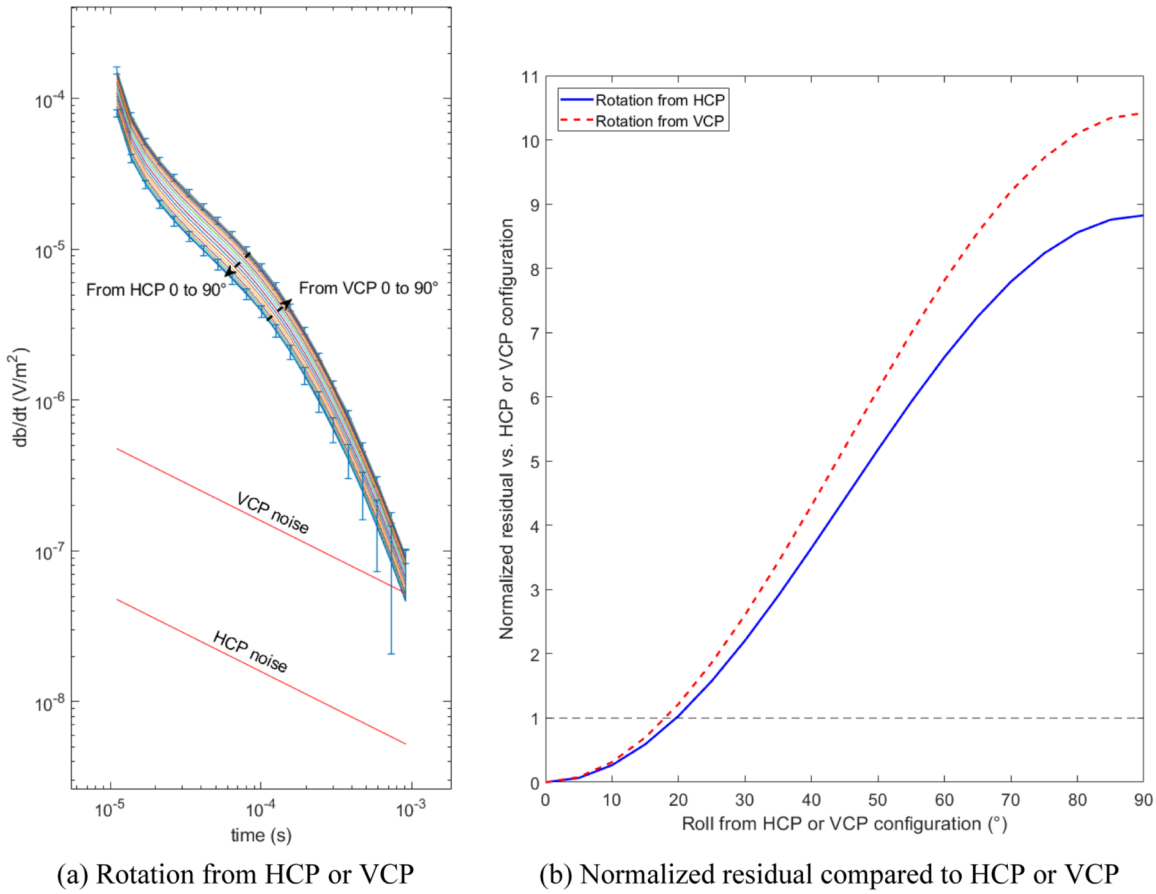

(a) Rotation from HCP or VCP (b) Normalized residual compared to HCP or VCP

FIGURE 7 (a) evolution of the TDEM response in function of the rotation angle; (b) normalized residual compared to the 0° orientation. Effect of the roll (rotation around *X* axis, cf. scheme in Figure 3b) for the horizontal co-planar (HCP) and vertical co-planar (VCP) geometries considering the configuration of Table 1 and the tabular ground of Table 2

>1 only at one sounding location (Figure 10). VCP is likely to provide two distinguished 3D bodies through inversion if the spacing is at least 40 m. Under this spacing, 3D inversion is likely to provide information regarding the presence of at least one global resistive inclusion.

Case of H_x component

With existing airborne TDEM systems, and in the case of delineation of 3D structures (for instance, in mining exploration), the H_x component is often measured in addition to the H_z component. Because H_x was zero for a tabular background in the centre of a horizontal T_x loop, a similar sensitivity study was run with the Rx coil located 40 m behind the centre of the T_x loop. Figure 11a shows the residual map obtained for the two 50-m side bodies separated by 50 m. Two different anomalies can readily be identified, with a more important response for one of the bodies owing to the asymmetry of the H_z–H_x configuration. This distinction is also more pronounced than that in the VCP configuration (Figure 9b). Figure 11b shows the profiles for different body spacing values. Compared to VCP (Figure 10b), anomalies are more delineated, and body responses start to merge at smaller separations, from 20 to 40 m for the VCP configuration. Figure 11c,d shows the results when considering 20-m side bodies. As for HCP and VCP configurations, those smaller sand units cannot be detected.

DISCUSSION

A turn-off ramp of 10 μs was considered for both the 1D and 3D sensitivity analyses (Figures 4–11). The turn-off ramp was the first key parameter for obtaining the best near-surface resolution possible. Schamper, Auken et al. (2014) showed an improvement in near-surface resolution when gates earlier than 10 μs were exploited (once the remaining system response was removed) with a turn-off ramp close to 3 μs. However, in that study, a helicopter-borne time-domain electromagnetic (TDEM) system with a flight altitude of 30 m was used. Sensitivity tests with the light fixed-wing configuration and acquisition height at 50 m were also carried out considering a turn-off time of 3 μs. However, no

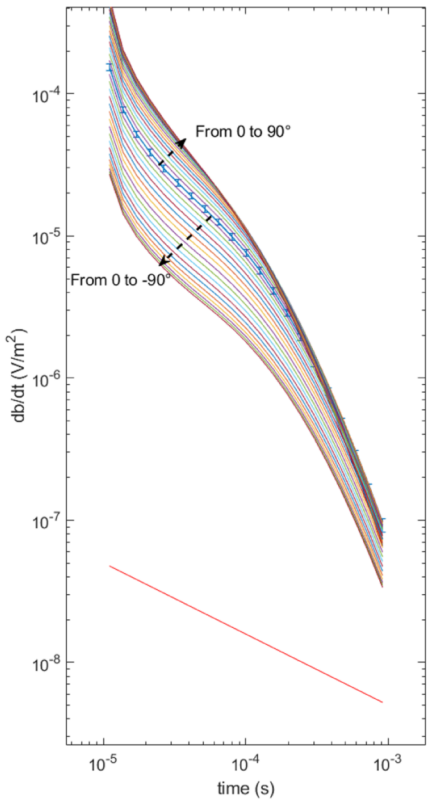

(a) Rotation from HCP

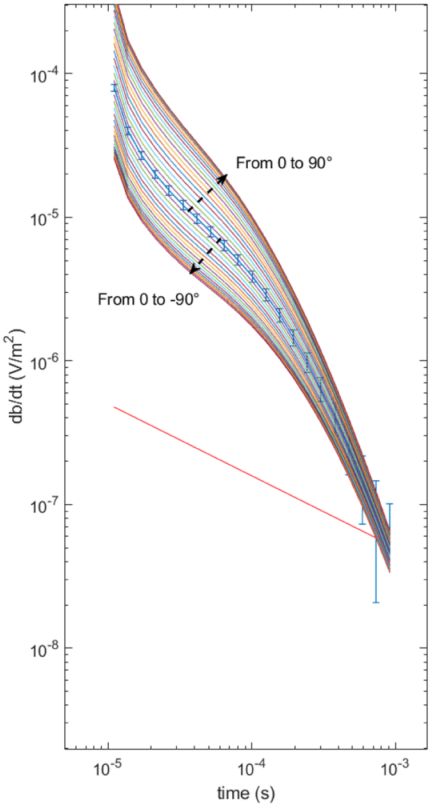

(b) Rotation from VCP

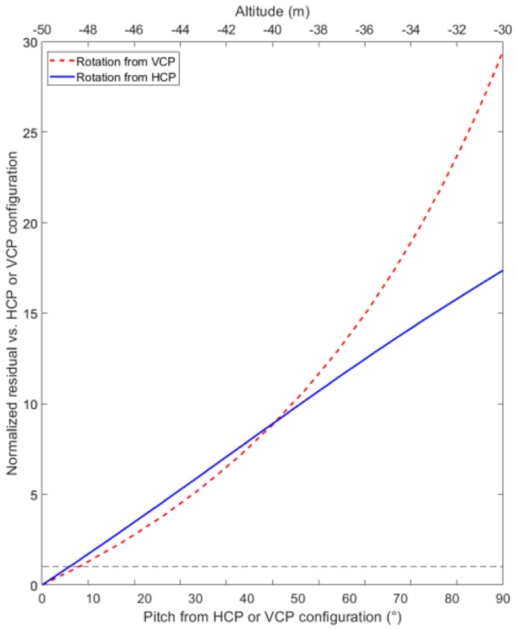

(c) Pitch with device tilting down

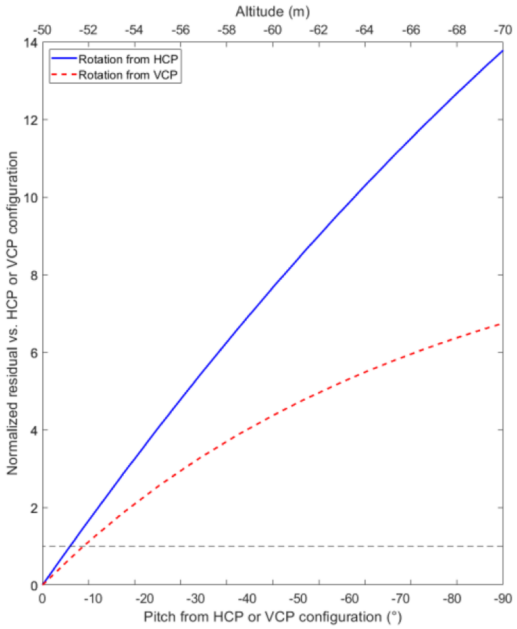

(d) Pitch with device tilting up

FIGURE 8 Effect of the pitch (rotation around *Y* axis, cf. scheme in Figure 3b) for the horizontal co-planar (HCP) (a) and vertical co-planar (VCP) (b) geometries considering the configuration of Table 1 and the tabular ground of Table 2. The normalized residual compared to the nominal HCP or VCP configuration (i.e. 0˚) is given in (c) for the device tilting down and in (d) for the device tilting up. Induced change in altitude is indicated on the top axis.

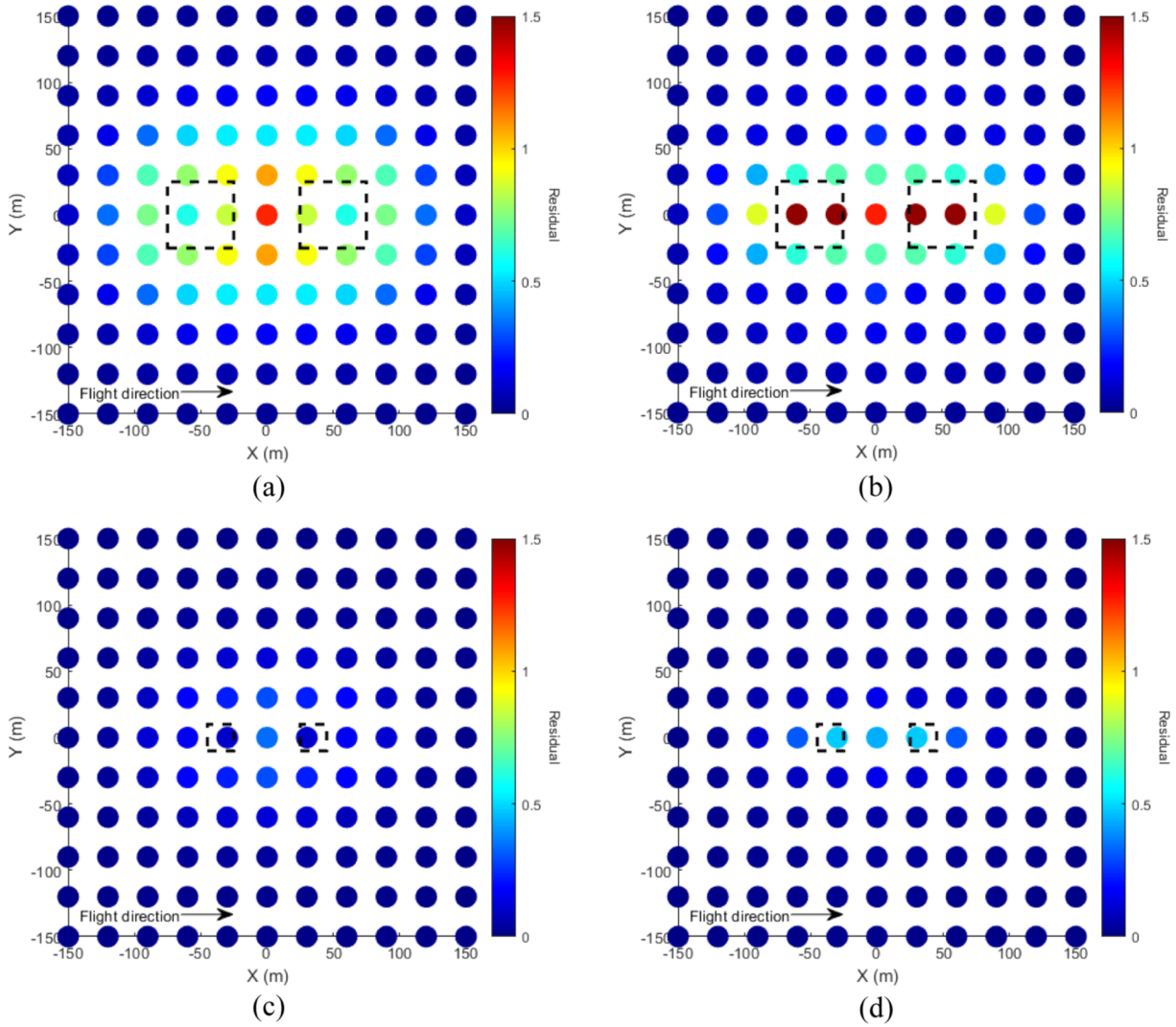

FIGURE 9 Residual maps for horizontal co-planar (HCP) and vertical co-planar (VCP) configurations with the 3D inclusions of 50 × 50 or 20 × 20 m^2 size as the ones shown in Figure 3 and separated by 50 m: (a) HCP and 50 x 50 m size; (b) VCP and 50 x 50 m size; (c) HCP and 20 x 20 m size; (d) VCP and 20 x 20 m size. The reference model is the same as in Figure 6 with a 5-m thick cover layer, without inclusions.

significant improvement in the near-surface sensitivity has been observed, likely due to the fact that the flight altitude of 50 m is already relatively large.

Even if the area of high residuals is larger for the vertical co-planar (VCP) than for the horizontal co-planar (HCP) (Figure 9a,b), this area is located along the *Y*-axis between −50 and 50 m. A flight line spacing of 50 m (which is dense and unusual for most airborne surveys) provides at least three flight lines where the responses of the 3D bodies are distinguishable from the background. For a line spacing above 50 m, it is likely that a single flight line will provide information, and no substantial response is measured at all for line spacings above 100 m. Therefore, a line spacing of a similar size to the 3D resistive inclusions to be mapped (whose response is weaker than those of conductive structures) is highly recommended when preparing the flight plan of the survey.

Although it has a lower signal-to-noise ratio (which is not a main issue when exploiting early times), the H_x component appears to be interesting for delineating near-surface lateral changes (Figure 11). However, co-planar T_x and Rx coils (in HCP or VCP configurations) are likely easier to tow, especially with a light fixed-wing airplane with limited power. This may be an aerodynamic limitation that needs to be evaluated.

Despite the effects of pitch and roll have been evaluated (Figures 7 and 8), non-planar deformations (e.g. undulations) of the T_x loop have not been modelled, which could have been an almost impossible task. However, such deformations have to be minimized as much as possible, as it can change the effective emission area and the coupling between the T_x and Rx coils, including the bucking coil whose purpose could be cancelled out, therefore making the exploitation of the early times for near-surface exploration impossible. Technical

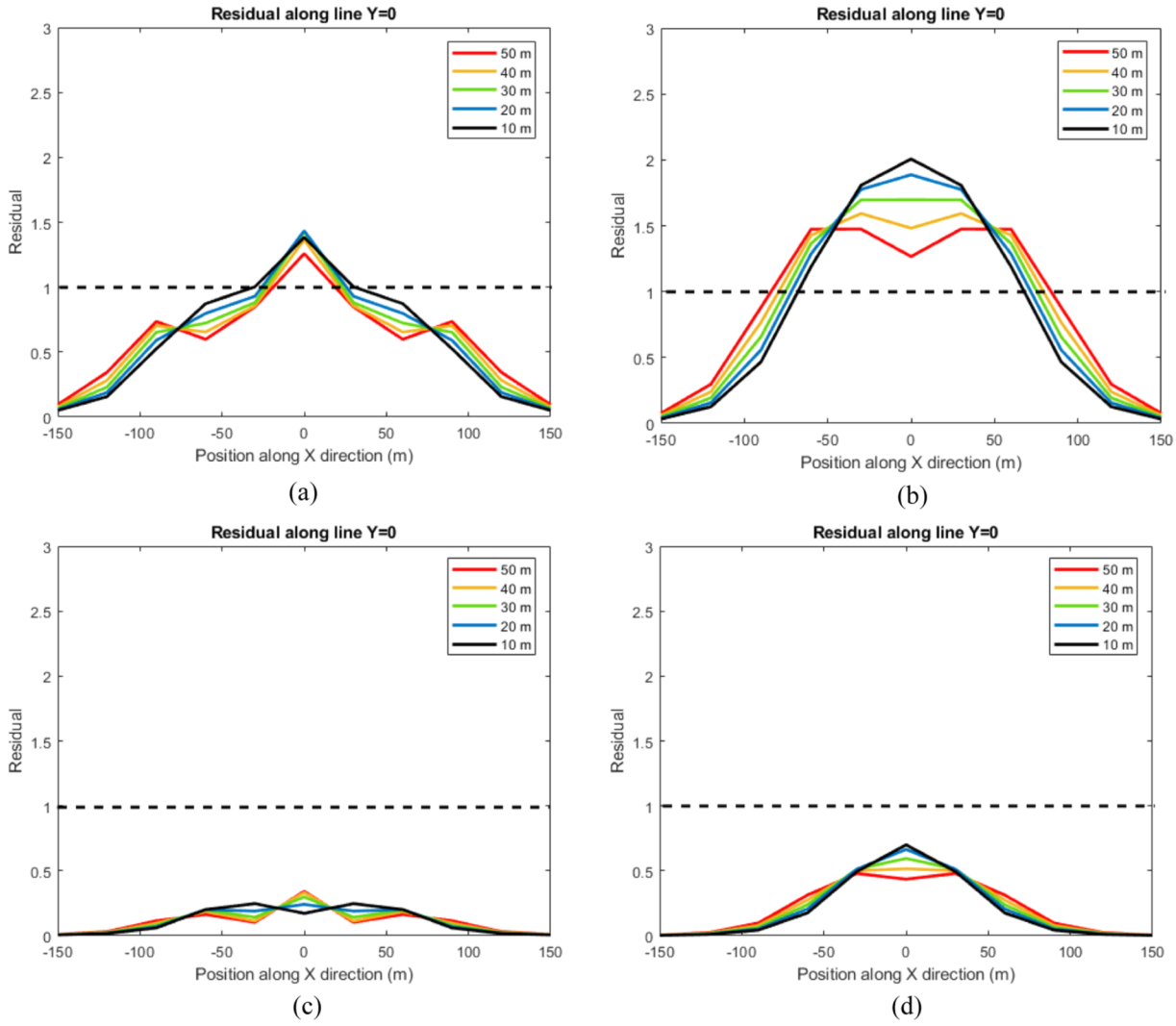

FIGURE 10 Residual profiles ($Y = 0$ m) across the 3D inclusions as the ones shown in Figure 3a and separated by a spacing varying from 10 to 50 m: (a) HCP and 50 x 50 m size; (b) VCP and 50 x 50 m size; (c) HCP and 20 x 20 m size; (d) VCP and 20 x 20 m size. The reference model is the same as in Figure 6 with a 5-m thick cover layer, without inclusions.

solutions to stiffen the T_x loop, while keeping it operable, are thus mandatory.

Head and tail winds between two consecutive flight lines are also likely to impact the position of the system in relation to the aircraft. GPS antennas set up on the T_x frame will help to accurately locate the device during the acquisition. The reduction of the T_x-aircraft distance as well as the intensity of the vibrations has to be monitored during field tests. If it appears that one flight line direction induces much more noisy data; therefore, survey with flight lines acquired in the same direction might be recommended.

The sensitivity results obtained are valid for the geological context considered (Orgeval basin, France), especially regarding the resistivity contrasts between a conductive (e.g. clayey) geological unit of approximately 10–30 Ω m and a more resistive (e.g. sandy) unit with resistivity above 50 Ω m, which corresponds to a particularly widespread plain alluvial context. Closer resistivity values between lithologies would result in much lower resolution capabilities, and new specific sensitivity studies following the same frame will have to be carried out in order to answer other geological contexts. For metric or even higher resolution of the cover layer, only ground-based surveys are able to provide information at such a small scale, such as the recent towed tTEM system (Grombacher et al., 2022), despite the fact that authorization for accessing agricultural parcels cannot be obtained depending on the period.

CONCLUSION

In the context of hydrogeomorphological mapping, a new airborne time-domain electromagnetic (TDEM) set-up with a light fixed-wing airplane is proposed. Despite the airplane being required to fly at a higher altitude, 50 m instead of

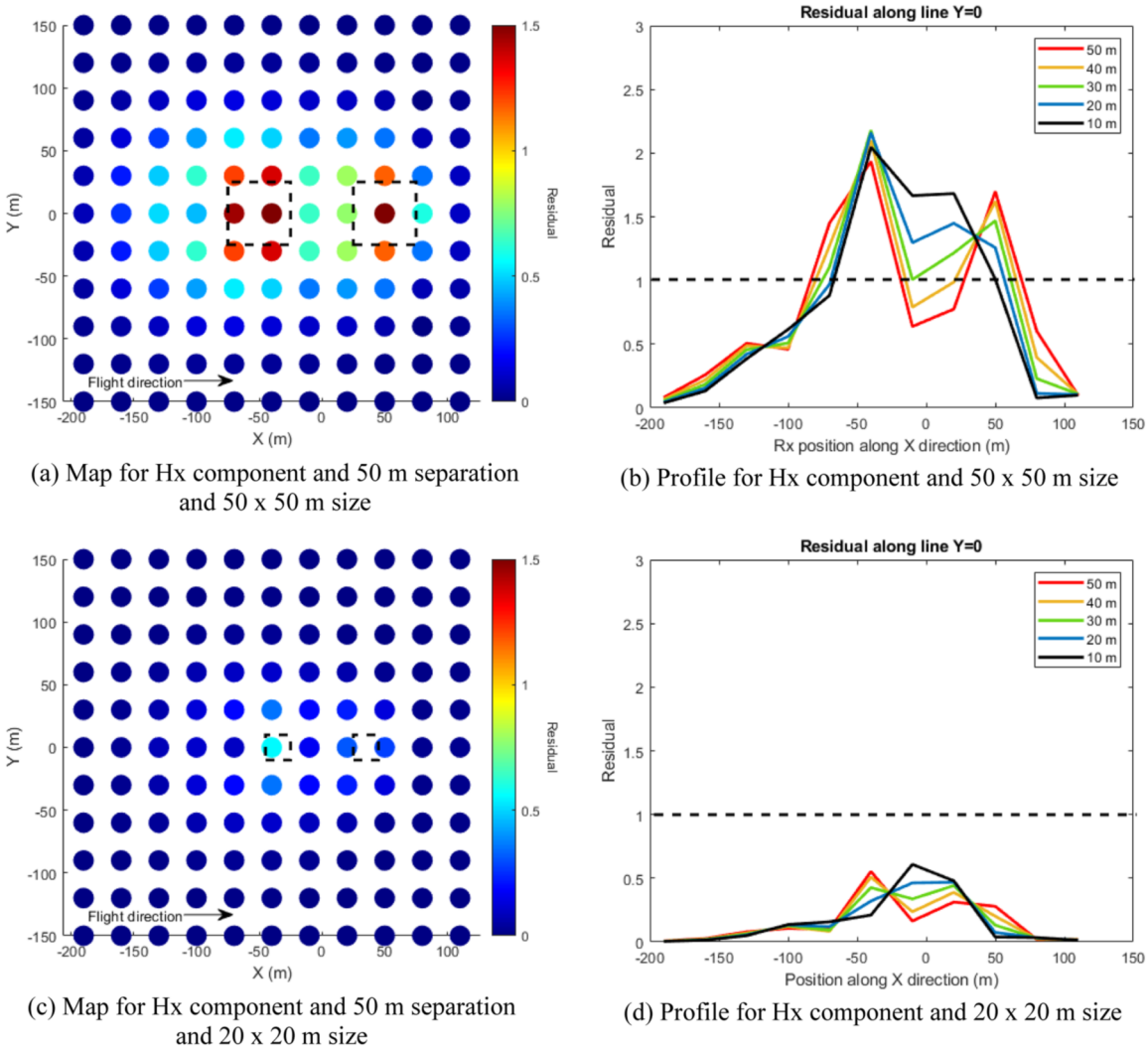

(a) Map for Hx component and 50 m separation and 50 x 50 m size

(b) Profile for Hx component and 50 x 50 m size

(c) Map for Hx component and 50 m separation and 20 x 20 m size

(d) Profile for Hx component and 20 x 20 m size

FIGURE 11 Residual maps (a and c) and profiles (b and d) when measuring H_x component with the Rx coil located 40 m behind the centre of the T_x horizontal loop (PERPxz configuration, cf. scheme in Figure 3b)

30 m with helicopter, the present sensitivity study focused on very near-surface formations in the first 5 m within a sedimentary context, in order to assess the detectability of the near-surface sandy or clayey cover layer which conditions the water infiltration from the surface to the aquifers. The airborne TDEM prototype also allowed the consideration of the vertical co-planar (VCP) geometry, which did not exist for TDEM systems of decametric size. Despite the analysis of the impact of some flight parameters on the sensitivity of the measurements, these analyses do not solve the practical and technical difficulties that will arise when making the system reliable and stable in air. However, the conclusions about the sensitivity to the near-surface ground parameters are encouraging.

In the 1D sensitivity analysis, it was concluded that the thickness of a few-meter conductive cover layer (15 vs. 40 Ω m for the underlying layer) could be mapped with a resolution of 2 m if the resistivity was constrained during inversion and if the thickness exceeded 1 m. For 1D interpretation, the VCP configuration did not provide better vertical sensitivity compared to horizontal co-planar (HCP) at a flying altitude of 50 m.

Regarding 3D mapping, decametric resistive inclusions ('hydraulic wells') of at least 50-m side could be detected, but the distinction between heterogeneities would have required spatial constraints/hypotheses from other datasets, especially for HCP (only if signal-to-noise ratio is high), whereas VCP data provided better spatial constraints by themselves (down to body spacing of ~40 m), but with the need for dense datasets. If aerodynamically compatible with a light fixed-wing airplane, the H_x component can allow the delineation of 50-m side bodies separated by a distance of at least 20 m.

ACKNOWLEDGEMENTS

We thank Quentin Vitale for participating in field campaigns. This research was funded by the TEMas project

(developed by PEGASE competitiveness), Action Air Environnement (S.A.S. Action Air Communication), the French Ministry of Higher Education and Research via CIFRE (Conventions Industrielles de Formation par la Recherche) funds, and the PIREN Seine program (Programme Interdisciplinaire de Recherche sur l'Environnement).

DATA AVAILABILITY STATEMENT

The data that support the findings of this study are available from the corresponding author upon reasonable request.

REFERENCES

Allard, M. (2007) On the origin of the HTEM species. In: *Proceedings of exploration: fifth decennial International Conference on Mineral Exploration*, vol. 7. pp. 355–374.

Anderson, W.L. (1982) *Nonlinear least-square inversion of transient soundings for a central loop system (Subprogram NLSTCI)*. Open-File Report, No. 82-1129. USGS. https://doi.org/10.3133/ofr821064

Auken, E., Foged, N., Christiansen, A.V. & Sørensen, K.I. (2007) Enhancing the resolution of the subsurface by joint inversion of x- and z-component SkyTEM data. In: *ASEG (Australian Society of Exploration Geophysicists) 19th geophysical conference, 18–22 November, Perth, Western Australia*. https://doi.org/10.1071/ASEG2007ab008

Bedrosian, P.A., Schamper, C. & Auken, E. (2016) A comparison of helicopter-borne electromagnetic systems for hydrogeologic studies. *Geophysical Prospecting*, 64(1), 192–215. https://doi.org/10.1111/1365-2478.12262

Christiansen, A.V. & Auken, E. (2012) A global measure for depth of investigation. *Geophysics*, 77(4), WB171–WB177. https://doi.org/10.1190/geo2011-0393.1

Cox, L.H., Wilson, G.A. & Zhdanov, M.S. (2012) 3D inversion of airborne electromagnetic data. *Geophysics*, 77(4), WB56–WB69. https://doi.org/10.1190/geo2011-0370.1

Effersø, F., Auken, E. & Sørensen, K.I. (1999) Inversion of band-limited TEM responses. *Geophysical Prospecting*, 47(4), 551–564. https://doi.org/10.1046/j.1365-2478.1999.00135.x

Fitterman, D.V. & Anderson, W.L. (1987) Effect of transmitter turn-off time on transient soundings. *Geoexploration*, 24(2), 131–146. https://doi.org/10.1016/0016-7142(87)90087-1

Finco, C., Pontoreau, C., Schamper, C., Rejiba, F., Hovhanissian, G., Calvez, R. et al. (2018) Towards a better understanding of near-surface aquifers in a saline and clayey environment with time-domain electromagnetic methods: Sebkha (salt lake) Kelbia, Tunisia. *Hydrogeological Processes*, 32(26), 3954–3965, https://doi.org/10.1002/hyp.13303

Fountain, D. (1998) Airborne electromagnetic systems – 50 years of development. *Exploration Geophysics*, 29(2), 1–11. https://doi.org/10.1071/EG998001

Grombacher, D., Maurya, P.K., Lind, J.C., Lane, J. & Auken, E. (2022) Rapid mapping of hydrological systems in Tanzania using a towed transient electromagnetic system. *Groundwater*, 60(1), 35–46. https://doi.org/10.1111/gwat.13130

Guillemoteau, J. & Tronicke, J. (2015) Non-standard electromagnetic induction sensor configurations: evaluating sensitivities and applicability. *Journal of Applied Geophysics*, 118, 15–23. https://doi.org/10.1016/j.jappgeo.2015.04.008

Guptasarma, D. & Singh, B. (1997) New digital linear filters for Hankel J0 and J1 transforms. *Geophysical Prospecting*, 45(5), 745–762. https://doi.org/10.1046/j.1365-2478.1997.500292.x

Hohmann, G.W. (1975) Three-dimensional induced polarization and electromagnetic modeling. *Geophysics*, 40(2), 309–324. https://doi.org/10.1190/1.1440527

Macnae, J. (2007) Developments in broadband airborne electromagnetics in the past decade. In: Proceedings of exploration: fifth decennial international conference on mineral exploration. vol. 7. pp. 387–398.

McNeill, J. (1980) *Electromagnetic terrain conductivity measurements at low induction numbers*. Technical Note TN-6. Geonics Ltd.

Mitsuhata, Y., Uchida, T., Murakami, Y. & Amano, H. (2001) The Fourier transform of controlled-source time-domain electromagnetic data by smooth spectrum inversion. *Geophysical Journal International*, 144(1), 123–135. https://doi.org/10.1046/j.1365-246x.2001.00324.x

Mouhri, A., Flipo, N., Rejiba, F., de Fouquet, C., Bodet, L., Kurtulus, B. et al. (2013) Designing a multi-scale sampling system of stream–aquifer interfaces in a sedimentary basin. *Journal of Hydrology*, 504(11), 194–206. https://doi.org/10.1016/j.jhydrol.2013.09.036

Munkholm, M.S. & Auken, E. (1996) Electromagnetic noise contamination on transient electromagnetic soundings in culturally disturbed environments. *Journal of Environmental and Engineering Geophysics*, 1(2), 119–127. https://doi.org/10.4133/JEEG1.2.119

Nyboe, N.S. & Sørensen, K.I. (2012) Noise reduction in TEM: presenting a bandwidth- and sensitivity-optimized parallel recording setup and methods for adaptive synchronous detection. *Geophysics*, 77(3), E203–E212. https://doi.org/10.1190/geo2011-0247.1

Sab, G.-A. (2017) Etude de faisabilité d'un dispositif TDEM aéroporté par avion léger, dans une perspective multi-capteurs. PhD Thesis.

Sab, G.-A., Schamper, C., Rejiba, F. & Tabbagh, A. (2014) Sensitivity analysis of a light fixed-wing airborne TDEM system for the characterization of karstic environments. In: Near surface annual meeting, 14–18 September, Athens, Greece. https://doi.org/10.3997/2214-4609.20142016

Sambridge, M. (1999) Geophysical inversion with a neighborhood algorithm—II. Appraising the ensemble. *Geophysical Journal International*, 138(3), 727–746. https://doi.org/10.1046/j.1365-246x.1999.00900.x

Schamper, C., Jørgensen, F., Auken, E. & Effersø, F. (2014) Assessment of near-surface mapping capabilities by airborne transient electromagnetic data – an extensive comparison to conventional borehole data. *Geophysics*, 79(4), B187–B199. https://doi.org/10.1190/geo2013-0256.1

Schamper, C., Auken, E. & Sørensen, K.I. (2014) Coil response inversion for very early time modeling of helicopter-borne time-domain EM data and mapping of near-surface geological layers. *Geophysical Prospecting*, 62(3), 658–674. https://doi.org/10.1111/1365-2478.12104

Schamper, C., Rejiba, F. & Guérin, R. (2012) 1D single-site and laterally constrained inversion of multifrequency and multicomponent ground-based electromagnetic induction data—application to the investigation of a near-surface clayey overburden. *Geophysics*, 77(4), WB19–WB35. https://doi.org/10.1190/geo2011-0358.1

Schamper, C., Rejiba, F., Tabbagh, A. & Spitz, S. (2011) Theoretical analysis of long offset time-lapse frequency domain controlled source electromagnetic signals using the method of moments: application to the monitoring of a land oil reservoir. *Journal of Geophysical*

Research: Solid Earth, 116(B3), B03101. https://doi.org/10.1029/2009JB007114

Siemon, B., Ibs-von Seht, M. & Frank, S. (2020) Airborne electromagnetic and radiometric peat thickness mapping of a bog in Northwest Germany (Ahlen-Falkenberger Moor). *Remote Sensing*, 12(2), 203. https://doi.org/10.3390/rs12020203

Smith, R.S. & Keating, P.B. (1996) The usefulness of multicomponent, time-domain airborne electromagnetic measurements. *Geophysics*, 61(1), 74–81. https://doi.org/10.1190/1.1443958

Sørensen, K.I. & Auken, E. (2004) SkyTEM – a new high-resolution helicopter transient electromagnetic system. *Exploration Geophysics*, 35(3), 194–202. https://doi.org/10.1071/EG04194

Sørensen, K.I., Mai, S., Mohr, K.R. & Nyboe, N.S. (2013) Development of high dipole TDEM systems. In: *SAGA (South African Geophysical Association) 13th biennial conference, 6–9 October, Mpumalanga, South Africa*. https://doi.org/10.3997/2214-4609-pdb.383.AEM2013_DAY1_SESSION_1A_Sorensen

Steuer, A., Siemon, B. & Auken, E. (2009) A comparison of helicopter-borne electromagnetics in frequency- and time-domain at the Cuxhaven valley in Northern Germany. *Journal of Applied Geophysics*, 67(3), 194–205. https://doi.org/10.1016/j.jappgeo.2007.07.001

Tabbagh, A. (1985) The response of a three-dimensional magnetic and conductive body in shallow depth electromagnetic prospecting. *Geophysical Journal International*, 81(1), 215–230. https://doi.org/10.1111/j.1365-246X.1985.tb01360.x

Tallec, G. (2012) 1962–2012: cinquante ans d'observations, un bien précieux pour la recherche et les services opérationnels. *Sciences Eaux Territoires*, 2012/III (Cahier spécial), pp.2–9. https://doi.org/10.3917/set.hs05.0002

Tallec, G., Ansart, P., Guérin, A., Delaigue, O. & Blanchouin, A. (2015) Données principales de l'observatoire ORACLE, Observatoire Oracle [Data set]. Irstea. https://bdoh.irstea.fr/ORACLE/

Thiesson, J., Tabbagh, A. & Flageul, S. (2007) TDEM magnetic viscosity prospecting using a Slingram coil configuration. *Near Surface Geophysics*, 5(6), 363–374. https://doi.org/10.3997/1873-0604.2007018

Thomson, S., Fountain, D. & Watts, T. (2007) Airborne geophysics—Evolution and revolution. In: Proceedings of exploration: fifth decennial international conference on mineral exploration, vol. 7. pp. 19–37.

Ward, S.H. & Hohmann, G.W. (1988) Electromagnetic theory for geophysical applications. In: Nabighian, M.N. (Ed.) *Electromagnetic methods in applied geophysics, Vol. 1: Theory*. Society of Exploration Geophysicists, pp. 131–311. https://doi.org/10.1190/1.9781560802631.ch4.

How to cite this article: Schamper, C., Sab, G.-A., Rejiba, F. & Flipo, N. (2022) Performance of light fixed-wing airborne time-domain electromagnetic system for mapping the near-surface cover layer in an alluvial plain context: A numerical study. *Geophysical Prospecting*, 1–17. https://doi.org/10.1111/1365-2478.13306